JET-P(95)17

Recent Progress in the Measurement and Analysis of ECE on JET

D V Bartlett, C Bishop[1], R Cahill[2], A McLachlan[1],
L Porte, A Rookes[3].

JET Joint Undertaking, Abingdon, Oxfordshire, OX14 3EA, UK.
[1] Dept of Computer Science, Aston University, Birmingham, B4 7ET, UK.
[2] Matra Marconi Space, FPC 320, PO Box 16, Filton, Bristol, BS12 7YB, UK.
[3] Imperial College of Science, Technology and Medicine, London, SW7 2BZ, UK.

Preprint of a paper to be submitted for publication in the proceedings of
EC9, the 9th International Workshop on ECE & ECRH

Recent Progress in the Measurement and Analysis of ECE on JET

D Bartlett, C Bishop[†], R Cahill[‡], A McLachlan[†], L Porte & A Rookes*

JET Joint Undertaking, Abingdon, Oxon. OX14 3EA, UK
[†] *Dept of Computer Science, Aston University, Birmingham B4 7ET, UK*
[‡] *Matra Marconi Space, FPC 320, PO Box 16, Filton, Bristol BS12 7Yb, UK*
* *Imperial College of Science, Technology and Medicine, London, SW7 2BZ, UK*

Abstract

Recent changes to the JET ECE diagnostic system have been made to accommodate the changing requirements of JET and to enhance further the measurement performance of the broad-band heterodyne radiometer. The radiometer frequency coverage has been extended, its spatial resolution has been improved and a technique for frequency selective sharing of radiation among its six mixers has been developed. An analysis of the limiting resolution of ECE measurements has been made, and applied to the determination of the optimum IF filter widths for the radiometer. These improvements and the resolution analysis are described, and some illustrative results are shown. A study of the feasibility of using neural networks to reduce the level of systematic uncertainty in the JET ECE data has been completed. The technique and the results are presented.

(1) Introduction

The JET ECE measurement system consists of three different instruments: Michelson interferometers, a 12-channel grating polychromator and a 72-channel heterodyne radiometer. Since the last overview presentations of the system at EC-6 [1] and EC-7 [2] the instrumental hardware developments which have taken place have been mainly concerned with improvements to the radiometer. The Michelson and polychromator have now reached a stable level of performance and are not undergoing any significant further development.

Changes have been made to the front-end of the system (antennas and windows) to accommodate the changing requirements of the JET machine. These are described briefly. The remainder of the paper concentrates on two other areas.

First, the radiometer frequency coverage has been extended so that it is now continuous from 73 to 139 GHz and its spatial resolution has been improved by the installation of a quasi-optical collection system and the addition of narrow-band intermediate frequency (IF) filters. To offset the reduced signal levels resulting from these changes, frequency selective beamsplitters (which improve the efficiency of the sharing of radiation among the six mixers in the radiometer) have been developed. The limiting resolution of ECE measurements due to relativistic broadening of the emission has been investigated, and has been applied to the determination of the optimum IF filter widths for the radiometer. The hardware changes are described and the resolution analysis is outlined. Some example results which illustrate the upgraded radiometer performance are presented.

Secondly, the conclusions of a study of the feasibility of using neural networks to reduce the level of systematic uncertainty in the JET ECE data are described. The method was described in detail at EC-8 [3]. It is recalled briefly here, and the results of the investigations are presented.

(2) Changes for the New Configuration of JET

During the major shutdown for the installation of the JET Mark I Pumped Divertor, which was completed in January 1994, major changes were made to the antenna configuration of the ECE system. New antennas were installed to adapt the diagnostic to the new JET configuration, in which the plasma centre is displaced upwards from the vacuum vessel midplane by typically 0.3 to 0.4 m, a quasi-optical collection system for improved antenna pattern for the radiometer was installed, and all vacuum windows were replaced with double-disc versions for improved reliability during future tritium experiments.

The fan array of antennas which had been used for measurements across the poloidal cross-section of the plasma [4] was removed and replaced with three horizontal antennas at heights 0.13, 0.25 and 0.35 m. These antennas are of the same design as existing array of horizontal antennas: from an aperture of 50 x 65 mm at the plasma end they taper, over a length of 1.5 m which includes (because of access constraints) a shallow bend, to 30 x 40 mm at the window. The radiation has free space propagation through the window to a 30 x 40 mm waveguide which then tapers up to the 34 x 73 mm WG10 (S-band) waveguide which is used to transport the radiation ~50 m to the measurement instruments. The in-vessel antennas are fabricated from Inconel and the external waveguides from high purity aluminium. The windows are z-cut crystal quartz. Combining the results of various calibration measurements gives an estimate for the transmission of this front-end assembly of ~50% in the range 100 - 200 GHz.

This new antenna array allows the grating polychromator, Michelson interferometer and heterodyne radiometer to operate simultaneously on sightlines generally close to the plasma centre. The radiometer can use either a conventional oversized horn antenna, or the quasi-optical (QO) collection optics described in the following section. The locations of all these sightlines is shown on a typical plasma cross-section in figure 1.

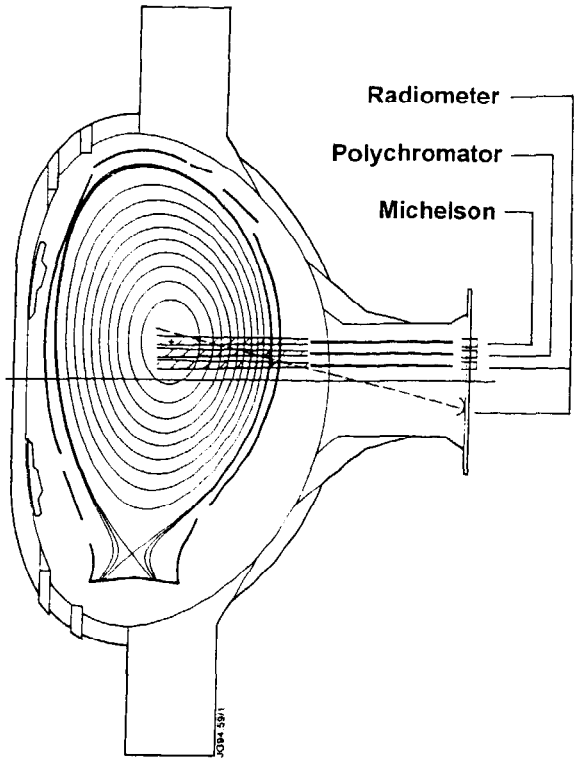

Figure 1: A poloidal cross-section of the new JET configuration, showing the location of the new ECE sightlines. The horizontal sightlines correspond to oversized waveguide antennas, while the sloping line corresponds to the view with the quasi-optical collection system for the radiometer.

(3) Performance Enhancements

The purpose of the performance enhancements to the radiometer is to be able to make electron temperature measurements over as much as possible of the plasma cross-section at all values of toroidal field used in JET, while simultaneously having the possibility of making T_e measurements with optimised spatial resolution. These changes (especially the use of narrow IF filters) lead to lower signal levels, so that the system noise can become comparable with the thermal noise of the black-body emission at temperatures of ~1 keV. To ameliorate this, frequency selective surface (FSS) beamsplitters have been developed for more efficient use of the radiation within the radiometer.

The spot size of the oversized waveguide antennas is about 0.2 m at the plasma centre. Hence, the spatial averaging of radiometer T_e measurements is dominated (for $r/a < 0.7$) by averaging over a range of flux surfaces rather than by radial resolution. A quasi-optical (QO) collection system has been installed to address this problem [5]. Its design is limited by several practical considerations: space available on and inside the main horizontal port flange, maximum window diameter, and the need to couple to the oversized waveguide used for transmission to the radiometer. Two concave mirrors are located on the vacuum side of the port flange, 0.13 m below the vessel midplane. An upward tilt of one mirror directs the sightline through the nominal plasma centre, as shown in figure 1. The mirrors focus onto a broad-band scalar feed horn outside the vacuum window. Following a short section of fundamental circular waveguide, which acts as a mode filter for both polarisations, the

radiation is re-launched into free space by an identical horn which is back-to-back with the first. A lens re-focuses the beam into oversized waveguide. The cross-polarisation of this assembly is calculated to be <25 dB, and the beam diameter is approximately constant across most of the outer half of the plasma, with 95% of the power within a diameter of about 80 mm, at 100 GHz.

To extend the frequency coverage of the radiometer, two further mixers have been added, bringing the total to six. The architecture of each of the six receivers is unchanged from that presented in [6]. However, the frequency coverage of the whole radiometer is now continuous from 73 to 139 GHz. The corresponding radial coverage, for first harmonic O-mode and second harmonic E-mode T_e measurements, as shown in figure 2, which plots the radial location of a measurement at fixed frequency as a function of central toroidal field. Each mixer appears as a diagonal band. The left group and the right group represent second and first harmonic measurements respectively. Second harmonic E-mode measurements are limited to an innermost radius of ~2.5 m by harmonic overlap. Since each mixer can be independently set to O- or E-mode, most of the outer half of the plasma can be measured at all fields used in JET. In fact, a subset of four of the six mixers provides sufficient radial coverage in almost all circumstances, and switches are used in the IF circuit (before the power splitters) to select two of the mixers from the group 1, 3 and 5, and two from the group 2, 4, 6. Hence, from the power splitters all the way through to the data acquisition, only four circuits (a total of 48 channels) are required.

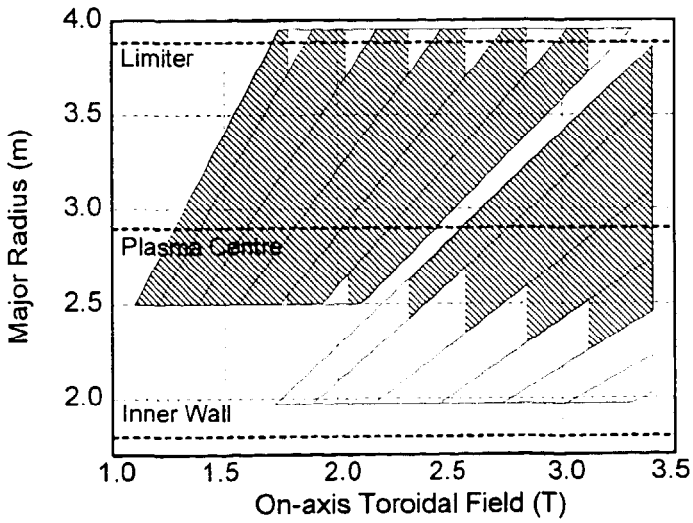

Figure 2: *The radial location of the cyclotron resonance for fixed frequencies, plotted as a function of the on-axis toroidal magnetic field strength. The variation of the radial coverage for each mixer in the radiometer, as a function of magnetic field, appears as a diagonal band. The six bands on the left correspond to second harmonic measurements, those on the right to the first harmonic.*

The radiation from one antenna and waveguide is shared between the six mixers by means of five beamsplitters as shown in figure 3. In the original four mixer system, coarsely wound wire grids were used as non-polarising beamsplitters [6]. Over the radiometer's frequency range there is little variation in the reflection and transmission of these grids, so in the new arrangement, each mixer receives typically 20% of the incident power. We have developed frequency selective surface (FSS) beamsplitters which provide a substantial

improvement over this. In the layout shown in figure 3, the first beamsplitter (on the plasma side) needs to reflect and transmit over the whole frequency range. However, for the other four beamsplitters, the allocation of mixers to waveguides has been chosen such that in each case the lower frequencies should be reflected, and there is a "dead-zone" of 12 GHz before the higher frequency region where transmission is required.

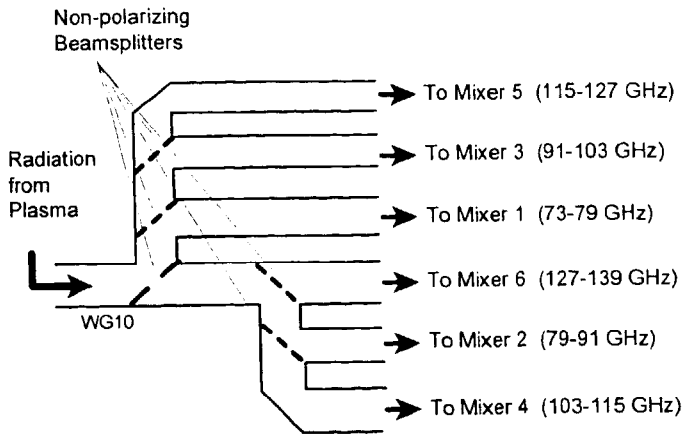

Figure 3: *The layout of the five beamsplitters used to share the radiation from a single waveguide among the six mixers. The first beam-splitter is not frequency selective, but the efficiency of use of radiation within the instrument is improved if the other four reflect lower frequencies and transmit higher frequencies. The layout ensures that for each beamsplitter there is a gap of 12 GHz between the required reflection and transmission zones.*

Very efficient FSS beamsplitters have been developed for other applications [7], but suffer limitations which make them unsuitable here: they operate near normal incidence, in free space, and usually for one polarisation only. The FSS beamsplitters developed for the JET radiometer [8] consist of a basic element which is two concentric rings, repeated in a rectangular array. A rigorous modal analysis technique is used to calculate the FSS performance and so to find the optimum dimensions. To date only one FSS, optimised for reflection below 79 GHz and transmission above 91 GHz, has been fabricated but the design calculations indicate that a simple scaling of dimensions should give comparable performance for the other edge frequencies. The mean diameters of the rings are 0.32 and 0.88 mm, and the array periodicity is 0.97 mm. The rings were etched from a 2μm thick layer of aluminium sputtered on a fused silica substrate of thickness 0.24 mm. Because of the large size required, rectangular areas were cut from three 60 mm diameter arrays, then bonded in precise alignment into a frame to form the beamsplitter, which is mounted in the waveguide in the same way as the wire grids [6].

Figure 4 compares the calculated (solid lines) and measured (squares) transmission of the FSS for both polarisations. The measured performance of a wire grid is also shown (open circles). The improvement over the wire grid is about a factor of two for the 73-79 GHz band, and somewhat less for the 91-103 and 115-127 GHz bands. If a similar performance is achieved with the other beamsplitters, then an average improvement over the whole frequency range of about a factor of two will be obtained. In practice, small adjustments to the parameters should allow more improvement to be made for those mixers generally used to

observe the weaker signals from near the plasma edge, at the expense of those mixers which generally measure near the plasma centre.

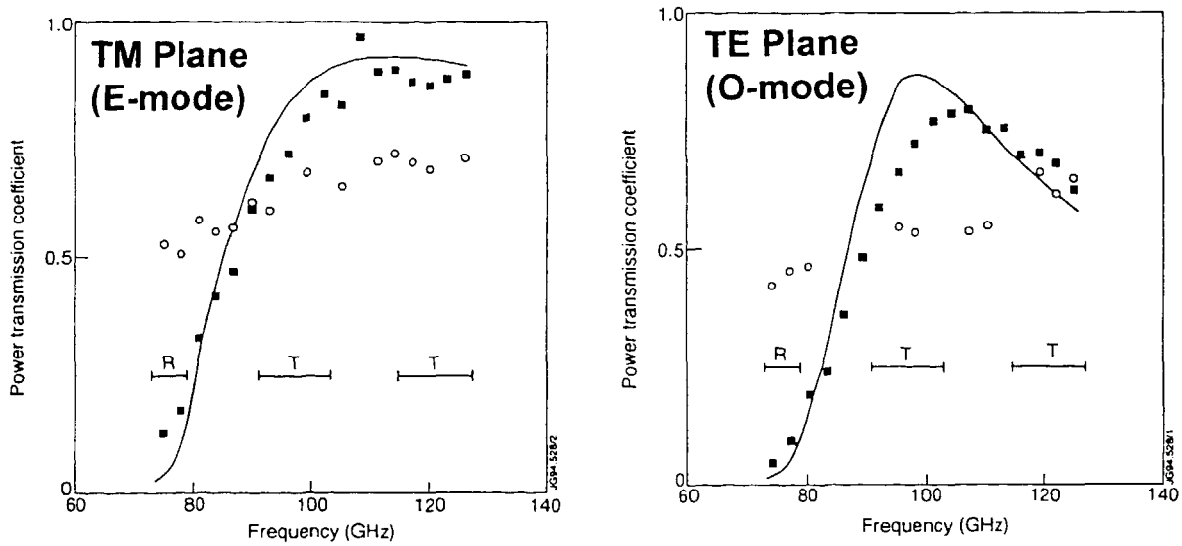

Figure 4: *Calculated (solid lines) and measured (squares) performance of the FSS beamsplitters, compared with the coarse wound wire grids (circles). Both polarisations are shown.*

Unlike the Michelson and polychromator instruments, where very high resolution is difficult to achieve at these wavelengths, the spectral resolution of the radiometer can easily improved by employing narrower IF filters. The performance of the instrument can therefore be optimised by choosing filter widths comparable to the fundamental limit set by spectral broadening of the ECE. Narrower filters would reduce the signal-to-noise ratio of the measurements without further benefit to the resolution. Filters of widths 100 to 250 MHz are a suitable lower limit for various conditions in JET, as discussed in the following section.

(4) Analysis of Limiting Spatial Resolution

In a hot plasma such as JET the spectral broadening of ECE is large, so that for a fixed frequency the cyclotron resonance can have a radial width of tens of centimetres. However, since the total optical depth of the first harmonic O-mode or second harmonic E-mode can be very large in JET (typically several tens) there is substantial re-absorption within the resonance. For observation from the outboard side and perpendicular to the magnetic field, only radiation emitted from a shallow layer on the outboard side of the resonance reaches the antenna. The effective radial resolution is therefore much less than the total width of the resonance. This effect can be calculated numerically by solving the radiation transport equation using well known expressions for the relativistic absorption coefficient, such as those in [9]. However, in order to have some simple criteria for the choice of IF filters in the radiometer, it is convenient to develop a semi-analytic approximation (applicable to the

second harmonic E-mode or first harmonic O-mode in the tenuous plasma approximation) for this effective radial resolution.

The observed emission intensity of a Maxwellian plasma can be obtained from the well known solution of the radiation transport equation:

$$I = \int_{-a}^{a} I_b(x)\alpha(x)e^{-\tau(x)}dx \qquad (1)$$

where I is the intensity of the emission, $I_b(x)$ is the local black-body intensity, $\alpha(x)$ is the local absorption coefficient, and $\tau(x)$ is the local optical depth, obtained by integrating $\alpha(x)$. We simplify this equation by assuming that T_e and n_e are constant within the emission region, so that I_b is constant and can be taken outside the integral. Moreover, the spatial variation of the emission and absorption is then all contained in the imaginary part of the F-function in the expression for $\alpha(x)$ [9], which we write in the form:

$$\alpha(x) = \kappa . \tau_{tot} . F''_{7/2}(z_m) \qquad (2)$$

where κ is a constant chosen to allow τ_{tot}, the total optical depth of the resonance, to be used as a normalisation factor. The argument of the F-function is $z_m = 511/T_e(1 - m\omega_c/\omega)$ (for T_e in keV). Taking I_b to the left side of Equation 1, we then have an expression for I/I_b in which the plasma parameters are contained τ_{tot} and the T_e dependence of z_m. The integrals of Equation 1 are calculated numerically for various values of τ_{tot} to determine the value of z_m for which I/I_b reaches some threshold value. For fixed frequency we can equate z_m with the spatial coordinate ΔR (=distance from the non-relativistic resonance radius, R, where $z_m = 0$):

$$z_m = (\Delta R/R).(511/T_e) \qquad (3)$$

Figure 5 shows the result of this calculation for I/I_b = 0.9. It can be viewed as illustrating the region from which 90% of the observed intensity originates, expressed as $\Delta R/R$ (normalised to T_e) as a function of total optical depth. It is apparent that for reasonably large values of optical depth (>15) the product $(\Delta R/R).(511/T_e)$ is a weak function of τ_{tot}.

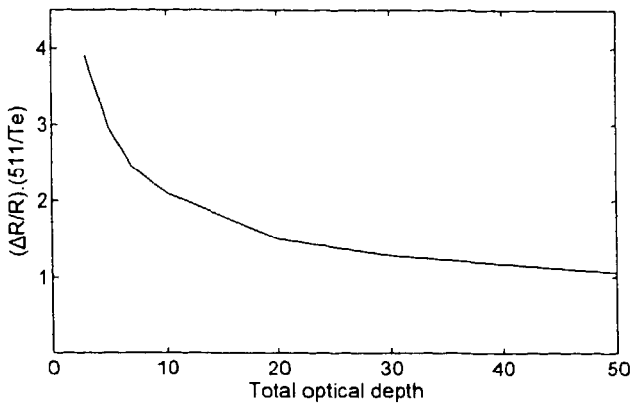

Figure 5: *Localisation of first harmonic O-mode or second harmonic E-mode emission (to the 90% level) expressed as $(\Delta R/R).(511/T_e)$ (with T_e in keV) as a function of the total optical depth of the resonance.*

The above analysis has been used to determine the radial resolution of the edge measurements shown in figure 6. With IF filters of width 100 MHz, radial resolutions of 10 mm are obtained. This allows the edge T_e gradient to determined with better precision than was previously possible. Gradients up to 100 keV/m have been seen in H-mode discharges.

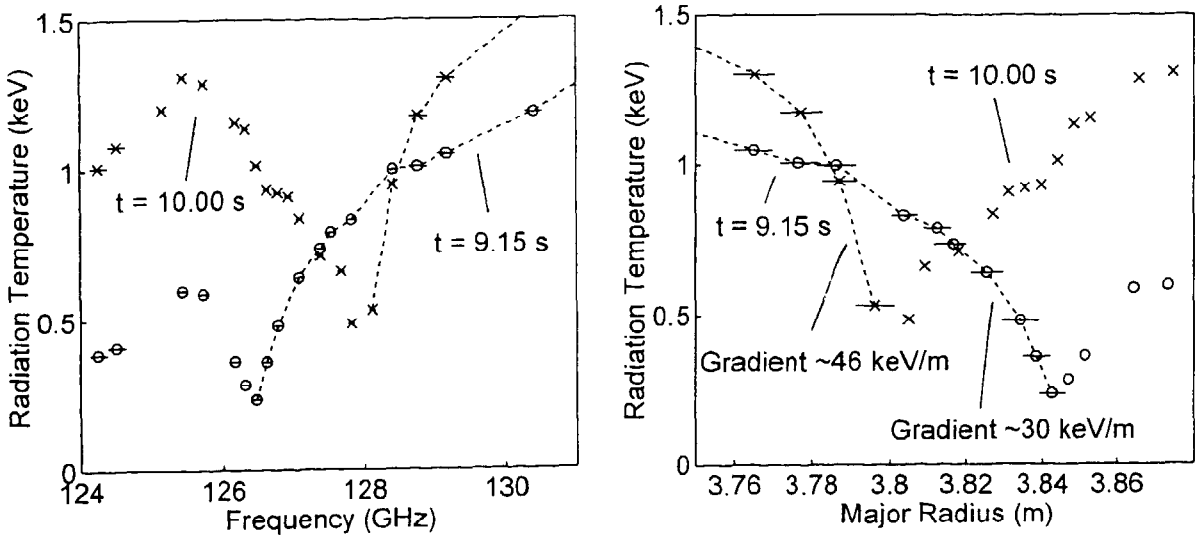

Figure 6: *High resolution edge measurements made with the heterodyne radiometer at two different times during an H-mode The left figure is in the spectral domain: each symbol is a radiometer channel with a horizontal bar to show the spectral resolution. A line connects the data points for which the T_e measurements are valid. In the right figure, the same data is plotted as a function of radius, with horizontal bars representing the radial resolution of each channel.*

(5) Application of Neural Networks to JET ECE Data

At the EC-8 Workshop, the first results of an investigation into the feasibility of using neural networks in the comparison of ECE and LIDAR Thomson scattering measurements were presented [3]. The purpose of this study is to attempt to reduce the two principal sources of systematic errors in the ECE T_e measurements: uncertainties in the spectral calibration and uncertainties in the calculated spatial profile of the total magnetic field strength. The LIDAR T_e profiles are believed to have low systematic errors and so are used as training data for the neural network. That is, the internal parameters of a network are adjusted so that it transforms the ECE data to resemble as closely as possible the LIDAR profiles. If the network structure has been suitably chosen, then it should produce similar improvements when confronted with new data. The reason for using neural networks for this purpose is that they have a powerful non-linear mapping capability, which should be able to correct the two sources of systematic error which are simultaneously present, but distort the ECE T_e profiles in different ways. This is difficult to do with conventional techniques.

It must be borne in mind that this technique does not introduce new physical understanding into the analysis of the ECE data: the "improvements" in the resulting ECE T_e profiles are due to a systematic modification which causes them to resemble more closely the LIDAR profiles, in a globally averaged sense. Any unknown systematic errors in the LIDAR data would therefore be transferred to the ECE profiles. The value of using this technique is that the lower random error and better time resolution of the ECE measurements are retained in the network outputs, while the systematic errors should be reduced.

A description of the application of neural networks to this problem, plus details of the implementation used for the JET data are given in the EC-8 paper [3]. In brief, a dataset of about 2000 simultaneously measured ECE and LIDAR T_e profiles, together with a selection of 10 parameters derived from magnetics measurements (toroidal field, plasma current, plasma elongation etc) is used. Each network has 23 input parameters (10 magnetics plus 13 ECE T_e values) and 11 outputs which match the LIDAR profile. Each network is trained on a subset of the 2000 profiles (the "training set"). Progress during training is monitored using another subset (the "validation set") and a third subset provides data which the network has not seen before for the final test of network performance (the "test set"). To quantify the improvement due to a trained network, its outputs for the test data set are compared with the "conventional" analysis of the same ECE data, ie profiles obtained from the ECE spectra by using a total magnetic field profile calculated from magnetics parameters. Several different measures of the agreement between ECE and LIDAR profiles have been used: the RMS difference between an ECE and a LIDAR profile (the "profile RMS error", as defined in Equation 3 of [3]) gives a profile-averaged indicator, while the average of this quantity over the whole test set (the "global RMS error", Equation 4 of [3]) provides a simple way to compare different networks. For the most detailed statistical analyses, the radial variation of the ratio of the two profiles has been used.

Two different types of network structure have been examined. The first uses a standard multi-layer perceptron network with a single hidden layer. Preliminary results from this network structure were presented at EC-8. A scatter plot of the profile RMS errors, comparing conventional with a typical network result, showed a general reduction in the errors of the network outputs relative to the conventional ECE profiles.

The complete study of this network structure includes the training of networks with different numbers of units in the hidden layer. Each network is trained 20 times, with random initial weights, and the results from the best training run are taken. When the number of hidden units is increased from 3 to 16, the global RMS error for the **training set** continues to fall, but for the validation set there is no improvement beyond about 7 hidden units, which suggests that the network is overfitting the training data. This is shown in figure 7. To investigate this further, a Principal Components Analysis (PCA) has been applied to the LIDAR profiles. In this analysis, the data are projected onto a new set of orthogonal axes, the first (principal) axis being chosen such that the maximum variance of the data lies along it, then the maximum variance in the remaining orthogonal directions is made to lie along the second axis, and so on. The global RMS error of a limited dimensionality representation determined in this way can be compared with the corresponding network error. It is found that

the global RMS error of a 7 dimensional representation of the LIDAR profiles is about half that of a 7 hidden unit network, and the PCA error continues to fall with increasing dimensionality, reaching zero at 11 dimensions. On different training runs the network error ceases to improve somewhere in the range 5 to 9 hidden units. We therefore conclude that at around 7 hidden units the global RMS error of the network outputs is determined by the characteristics of the ECE and LIDAR measurements and not by the limited dimensionality of the network. The outputs of networks with 7 hidden units have been used in the following analyses.

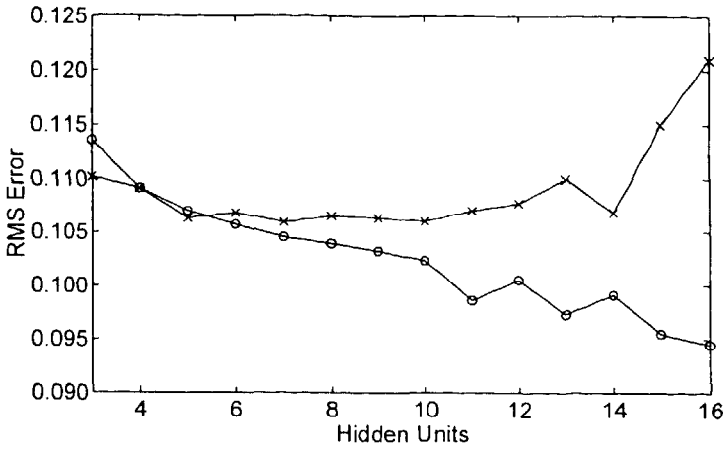

***Figure** 7: The global RMS error for networks with different numbers of units in the hidden layer. The circles are results obtained on the training data, while the crosses are the result of applying the same networks to the validation data set. The apparent improvement with many hidden units during training is not seen on the validation data set. These curves show some "noise", due to the limited number of training runs used.*

The sensitivity of the network improvements to the various input parameters has been studied by suppressing each of them in turn and comparing the global RMS errors of the re-trained networks. Of the 10 magnetics parameters in the input data, the network performance is most sensitive to the plasma current and the elongation of the boundary, with the triangularity of the boundary and elongation at the plasma centre being of least importance.

The network performance has been characterised in more detail by dividing the major radius range from plasma centre to edge into four bands, labelled "A" (2.8 - 3.0 m, ie. around the plasma centre), "B" (3.1 - 3.3 m), "C" (3.4 - 3.6 m) and "D" (3.7 - 3.8 m, ie. closest to the edge). Within each band the average T_e(LIDAR)/T_e(ECE) is calculated for each profile. The statistical behaviour of these ratios, for both conventional and the best 7 hidden unit network analyses have been compared.

The simplest analysis is to make histograms of the ratio values, as shown in figure 8. In the upper part of the figure, the histograms for the four radius bands with the conventional ECE profiles show that the mean ratio is ~0.9 (as has been seen in previous ECE/LIDAR comparisons), the standard deviation of the distribution is ~0.1 near the plasma centre rising to ~0.2 near the edge (in both cases larger than the LIDAR statistical error), and the distributions become asymmetric near the plasma edge. The network outputs, however, have unity mean, a standard deviation for the radius ranges A, B and C of 0.07 to 0.08 (consistent with the usual LIDAR statistical error of ~0.07), and much less asymmetry.

The systematic variation of the LIDAR/ECE ratio with the magnetics parameters has also been investigated. As an example, figure 9 shows the ratios in each of the four radius bands as a function of plasma current, for the conventional and network outputs. By eye, there

appears to be a trend for the A and B radius ranges in the conventional results which is removed by the network. This can be quantified by performing a standard statistical test on the

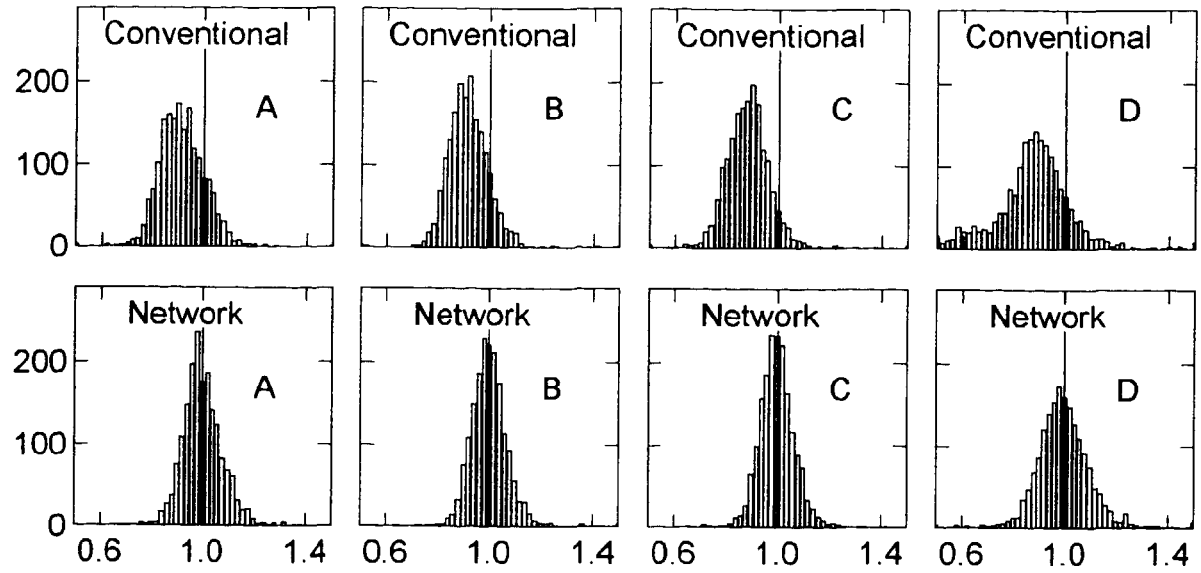

Figure 8: *Histograms of the distribution of the LIDAR/ECE ratios in the four radius ranges, for both network and conventional analyses. The network outputs shown reduced spread and better symmetry of the distribution.*

linear correlation coefficients for this data. The correlation coefficient between a set of ratios and the corresponding values of the magnetics parameter is calculated using the standard formulae and then transformed into a random variable from the t-distribution [10]. If this value, denoted t, satisfies $|t| > 1.96$ then we can say with 97.5% confidence that there is a correlation. Table I shows values of t for a selection of the magnetics parameters. Absolute values greater than the 1.96 threshold are highlighted: they are almost all in the left half of the table, ie. corresponding to the conventional analysis. There are few examples of statistically significant correlation for the network profiles, and these in radius band D, near the plasma edge.

TABLE I: Values from the t-distribution for conventional and network profiles, showing the systematic correlation with various magnetics parameters.

	Conventional Profiles for radius range:				Network Profiles for radius range:			
Parameter	A (centre)	B	C	D (edge)	A (centre)	B	C	D (edge)
Toroidal field	-0.548	**-4.187**	-0.754	**-11.783**	-0.193	-0.216	-0.925	-0.621
Plasma Current	**-4.325**	**6.478**	1.029	**18.936**	0.648	-0.108	1.563	-0.457
Toroidal β	**15.849**	**8.026**	-1.052	**-6.018**	-0.395	-1.240	0.435	**1.972**
Inductance (l_i)	**-8.365**	**-2.621**	0.424	**11.071**	0.903	0.351	1.535	**-2.915**
Ellipticity	**9.221**	**2.100**	-1.112	**-12.958**	-0.300	0.479	0.475	1.312
Triangularity	**7.937**	**5.109**	-0.694	**-3.228**	0.399	0.817	1.198	1.007

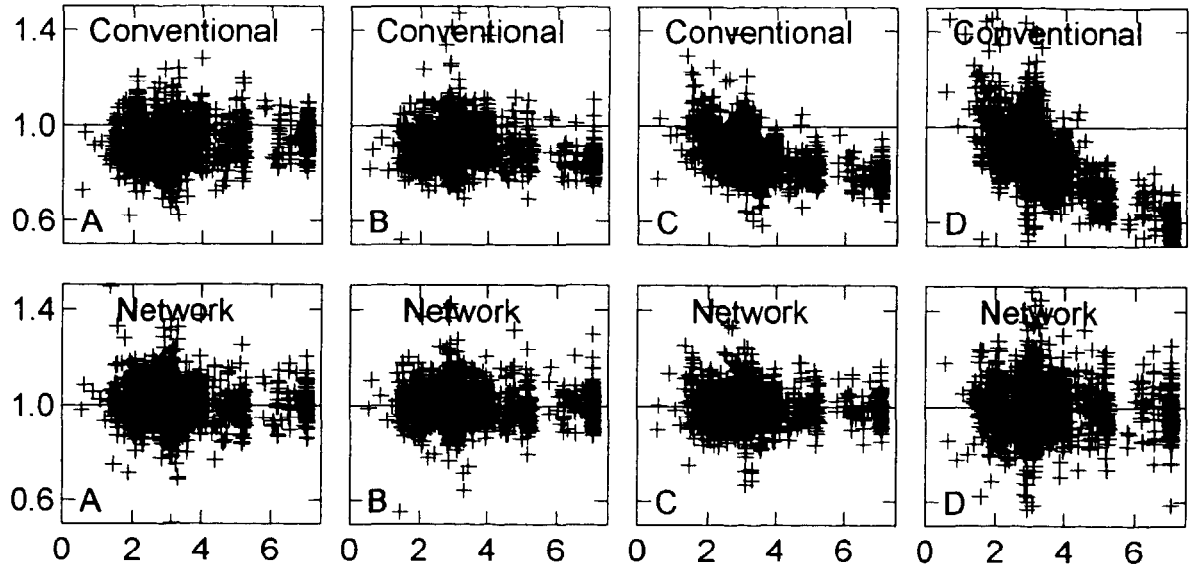

Figure 9: *Scatter plots of the LIDAR/ECE ratio against plasma current (in MA). A systematic variation of this ratio with current is visible in the results of the conventional analysis, especially towards the plasma edge (radius ranges C and D). This correlation is not present in the network outputs.*

The second network structure which has been investigated attempts to exploit our understanding of the sources of systematic error in the ECE data. Two networks are used [3]: one scales the ECE spectra to remove calibration errors, the other modifies the vacuum magnetic field profile by adding a polynomial in R. It was expected that this structure would give better results than the first, as well as providing access to useful information about calibration errors and (possibly) the magnetic field profile. In fact, it has been found that while there is still significant improvement over the conventional analysis, the results obtained are slightly poorer than those from the first network structure. The exact reasons for this are still being investigated, but it seems that although the network generates reasonable calibration corrections, the magnetic field profiles which are produced are not reliable.

The next steps in this investigation will be to probe further into the reasons why the second structure performs poorly, and to adapt the analysis so that it can be applied to current JET data. Allowance will have to be made for the fact that the new ECE sightlines are well separated from the LIDAR sightline (which remains on the vacuum vessel midplane), especially since the vertical position of the plasma centre varies over a wide range.

(6) Summary

As well as the modifications required to adapt the JET ECE system to the changing requirements of the JET machine, changes have been made to the heterodyne radiometer which have resulted in a further substantial improvement in its measurement performance. The wide frequency coverage allows T_e measurements across almost all the outer half of the plasma at almost all toroidal field values used in JET. The use of very narrow IF filters for edge measurements with radial resolution at the fundamental limit set by the ECE physics has been demonstrated. The simultaneous use of frequency selective beamsplitters to share more efficiently the radiation among its six mixers offsets the reduction in signal to noise ratio which results from the introduction of more mixers and narrower filters.

The study of the feasibility of using neural networks to reduce the level of systematic uncertainty in the JET ECE data has shown that T_e profiles which match more closely those produced by LIDAR can be obtained. Moreover, at the same time spurious correlations between the ECE temperatures and various plasma parameters (largely due to errors in the magnetic field profile used in the conventional analysis) can be eliminated. Further work is required to apply this analysis to current JET data.

Acknowledgements

The authors wish to thank R Wylde for his contribution to the design of the quasi-optical collection system, G Whitfield and D Wilson for their work on the new antennas and windows, and H Oosterbeek and I Hurdle for their continuing excellent technical support.

References

[1] "Overview of JET ECE measurements"; D V Bartlett et al. Proceedings of the Sixth International Workshop on ECE and ECRH (Oxford, 1987)

[2] "Recent developments in ECE measurements at JET"; A E Costley, et al. Proceedings of the Seventh International Workshop on ECE and ECRH (Hefei, China, 1989)

[3] "Development of neural network techniques for the analysis of JET ECE data "; D V Bartlett, et al. Proceedings of the Eighth International Workshop on ECE and ECRH (Gut Ising, Germany, 1992)

[4] "Measurement of two-dimensional temperature profiles in JET and simulation of the spectra"; S Nowak, et al. Proceedings of the Sixth International Workshop on ECE and ECRH (Oxford, 1987)

[5] "A broad-band QO collection system for the JET ECE heterodyne radiometer "; L Porte et al. Proc of the 18th Intl Conf and mm Waves (Colchester, UK, 1993)

[6] "The JET ECE heterodyne radiometer and investigation of fast phenomena"; D V Bartlett, et al. Proceedings of the Eighth International Workshop on ECE and ECRH (Gut Ising, Germany, 1992)

[7] "Frequency selective surface design for submillimetric diplexing"; R Cahill & E Parker, Microw. Opt. Technol. Lett., 7, 595 (1994)

[8] "Millimetric FSS waveguide beamsplitter"; R Cahill et al. Electronic Letters, **31**, 47 (1995)

[9] "Electron cyclotron emission and absorption in fusion plasmas"; M Bornatici et al. Nucl. Fusion, **23**, 1153 (1983)

[10] for example, "Statistics", M Spiegel (McGraw Hill Inc, 1992)